Gear mesh stiffness of polymer-metal spur gear system using generalized Maxwell model

Ala Eddin Chakroun[1,2], Chaima Hammami[1], Ahmed Hammami[1], Ana De-Juan[2], Fakher Chaari[1], Alfonso Fernandez[2], Fernando Viadero[2], Mohamed Haddar[1]

[1] Mechanics, Modelling and Production Laboratory, National School of Engineers Sfax, Tunisia

[2] Department of Structural and Mechanical Engineering, Universidad de Cantabria, Spain

Abstract

Polymer-metal gears become increasingly interesting to manufacturers and researchers for their advantages to combine the two material's efficiencies. Despite the variety of studies in the literature, there is a significant drop in the number of studies concerning the Gear Mesh Stiffness (GMS). The variation of the GMS by time has a major influence on the dynamic response of transmission. Therefore, this study proposes to take into consideration the viscoelastic behaviour of polymer in order to model effectively the GMS of a gear system. The suggested rheological model is the Generalized Maxwell Model (GMM). It is first used to model the viscoelastic behaviour of the plastic material of the pinion. Then, Pole Zero Formulation (PZF) is employed to identify parameters of the proposed model. A numerical simulation is then carried out to illustrate the results of this new approach adopted on a pure Nylon 6,6-steel pinions. The evolution of the GMS is illustrated to highlight the viscoelastic behaviour's model presented in this paper. Finally, the influence of the change in the temperature is investigated.

Keywords: Gear mesh stiffness, generalized Maxwell model, recovery, viscoelastic behaviour, spur gear, pole-zero formulation

1. Introduction

The importance of polymer gears for the transmission of power and motion is increasing due to their intrinsic material's characteristics. Therefore, they have emerged as competitive alternatives to traditional metal gears in a wide range of applications for their manufacturing cost reduction, their ability to reduce the high sliding occurring in the mesh and their self-lubrication. These several advantages are associated to the viscoelastic behaviour of the material that cannot be described with Hook's law which make it an interesting subject. In the review made by Singh et al. (Singh et al., 2018), it is mentioned that most researchers focused on design features (Kim, 2006)(Imrek, 2009)(Düzcükoğlu et al., 2010) and performance characteristics (Mao et al., 2009) (Li et al., 2011)(Mertens & Senthilvelan, 2016) of polymer gears. These studies are mainly based on an experimental approach and only few studies used simulation and numerical aspects. In addition, in the review made by Marafona et al. (Marafona et al., 2021), it is mentioned that there is minimum diversity on the models used to simulate the GMS of polymer gears. Furthermore, the majority of these models are finite element models, and few analytical ones were implemented. A numerical simulation of the GMS will thus bring an interesting addition in the field of polymer gears. But first, it is preferable to understand the viscoelastic behaviour of polymers and to propose an appropriate model to be used in this study.

The viscoelastic behaviour of polymers is usually modelled using rheological models. Two categories of models were developed where they represent the relation between stress and strain.

The first category of derivative fractional models were proposed by Bagley and Torvik (Bagley & Torvik, 1985) after being developed by mathematicians interested in fractional derivatives. The goal is to establish relation of fractional derivation between stress and strain. It can match the behaviour by using less parameters. A new element called "spring-pot" is thus proposed whose behaviour is between that of a pure spring and that of a pure shock absorber. In this context, the second one represents the relation strain-stress in the form of an assembly of springs and dashpots. Springs characterize material's elasticity and dashpots characterize its viscosity. In this category, there are simple models and more complex ones called generalized models. The generalized ones are the assembly of a finite number of cells in series or in parallel. Each cell is composed of a spring in series or in parallel with a dashpot. The number of elements used to effectively model material behaviour using generalised models can increase rapidly. It can thus result in the identification of an important number of parameters. Regardless of this main drawback, this category of models, specially the generalized ones, can usually be used to a better and more precise modelling of viscoelastic behaviour (Jrad et al., 2013). Therefore, one of them is going to be used in this study.

These models however are characterized by the following moduli. The storage modulus represents the elastic behaviour of the structure, and the loss modulus represents the viscous one (Ganeriwala & Rotz, 1985). The stress can be put into a form of Fourier series expression which depends on these moduli. Eventually, Stress-strain (Blanc & Ravasoo, 1996), creep (Almagableh et al., 2008), or recovery (Joo et al., 2007) curves can be determined. There are also primitive models to simulate viscoelastic behaviour where the most common are Maxwell and Kelvin-Voight. Derivatives from those models are also developed in the literature (Mainardi & Spada, 2011). Maxwell model is composed of a spring and a dashpot in series while Kelvin-Voight is composed of a spring and a dashpot in parallel. As mentioned earlier, generalized models allow for better viscoelastic modelling, with the following models being the most commonly used. GMM is combination of Maxwell cells in parallel and Generalized Kelvin-Voight model (GKM) is a combination of Kelvin-Voight cells connected in series. The former is generally used to determine the relaxation, storage and loss moduli, while the latter is generally used to determine the creep, storage and loss compliances. Formulas are established to find equivalence between these models (Serra-Aguila et al., 2019). Both models can thus give similar results but given the ability of the GMM to give the moduli directly, it is the one chosen for this study.

The goal of the work developed through this paper is to effectively model the GMS of a gear system by considering the viscoelastic behaviour. However, the GMS is the most commonly studied parameter when it comes to vibration analysis in gear systems. When it is modelled properly, it can give more advanced and reliable analysis tools to be used in industry 4.0. In the literature, many approaches were developed to model the meshing stiffness of metallic spur gears such as empirical formula (Henriot, 1985), approximation factors (International standard ISO 6336), numerical approach (Chaari et al., 2009) Finite Element Analysis (FEA) (Fernandez Del Rincon et al., 2013)…. Other studies have modelled the GMS of several gear types with different geometries, such as spur gears (Cui et al., 2019)(Farhat et al., 2020), helical gears (Walha et al., 2011)(Han & Qi, 2019), bevel gears (Driss et al., 2014)(Sun et al., 2019), worm gears (Chakroun et al., 2021) and planetary gears (Shen et al., 2020).

While there are numerous studies on GMS in metallic gears, there is a significant gap on polymer ones. The variation of possibilities of modelling the viscoelastic behaviour in the literature is enormous and the choice of an appropriate model is difficult. This behaviour of polymeric

materials is treated by many researchers. The study of Meuleman et al. (Meuleman et al., 2007) used a FEA code called "mechanical event simulation" that allows the modelling of a dynamic system. The authors studied the contact between a pair of gears with the same polymer (POM) material and a pair of gears with different materials, metal (steel) and polymer (POM). The mesh stiffness is then deduced from the bending deflection equation using the value of Young's modulus, which is not the case for polymers. The study of Lin and Kuang (Lin & Kuang, 2008) also modelled polymer gears using FEA model. But modelling the GMS was totally different from the ones mentioned previously. It is described by a numerical approximation based on curve-fitted coefficients for Nylon 6,6. Similarly, analytical results are obtained for POM gears with a relation derived from Nylon 6,6 approximation. The meshing stiffness is position-dependent and its variation due to the operating time influenced by viscoelasticity is not taken into account. One other approximate approach was developed in the study of Hasl et al. (Hasl et al., 2017). The method is abbreviated to the acronym "ACORA" meaning "**a**ctual **co**ntact **ra**tio". The calculation of the mesh stiffness used constant factors from DIN 3990. Then, by analogue parametrization, it is proposed to adapt a modified GMS to ACORA mesh stiffness. Finally, this mesh stiffness is a fluctuation between a maximum and a minimum number, which means that the viscoelastic behaviour has not been considered. Other researchers considered meshing stiffness related parameters (i.e., transmission error)(Tsai & Tsai, 1997)(Kodeeswaran et al., 2017) but without considering the time varying GMS. One can mention the work of Hiltcher et al. (Hiltcher et al., 2006) who investigate the load sharing in gear teeth using GKM. The use of GKM is also mentioned in other polymer gear studies (de Vaujany et al., 2008)(Cathelin et al., 2015). Yet, these studies did not show the influence of the viscoelastic behaviour on the GMS signal. As a conclusion, it is important to model the viscoelastic behaviour using a proper rheological model in order to study its influence on the GMS of a gearing system.

Eventually, it can be deduced that literature showed a lack in using rheological models to simulate the viscoelastic behaviour of polymers in gear applications. It is important to introduce them to simulate the behaviour of this type of materials. In this paper, the objective is to model the polymer using the GMM rheological model which is ideal for harmonic steady state excitation (Jrad et al., 2017) which is the case of gear teeth. Thus, GMM is used to model pure Nylon 6,6 as material of the gear running against a steel pinion to eventually deduce the GMS of this proposed spur gear system. The identification method for GMM parameters used here is pole-zero formulation (PZF). Eventually, the strain of one tooth of the polymer gear for one and multiple cycles is modelled. From this strain, the meshing stiffness of one tooth is determined. An overlay is then performed to deduce the GMS signal. Finally, the influence of viscoelastic behaviour and temperature on this signal is illustrated.

Nomenclature

Z	Impedance	w	The face width of a tooth
ω	The angular frequency	F	The load applied by the steel pinion
n	GMM number of cells	F_t	The tangential load applied by the steel pinion
E_∞	GMM equilibrium modulus	δ_c	The contact deflection of the Nylon 6,6 gear
E_i	GMM $i$est spring elastic modulus ($i \in [1\ n]$)	δ_b	The Bending deflection of the Nylon 6,6 gear

η_i	GMM $i$est dashpot viscosity ($i \in [1\ n]$)	h	The thickness of teeth contact
$\omega_{z,i}$	$i$est zero ($i \in [1\ n]$)	l	The chordal thickness of a tooth
$\omega_{p,i}$	$i$est pole ($i \in [1\ n]$)	e	The strain value of non-recovered material
$T_{z,i}$	Period of the $i$est zero ($i \in [1\ n]$)	ε_{creep}	Creep-strain
$T_{p,i}$	Period of the $i$est pole ($i \in [1\ n]$)	$\varepsilon_{recovery}$	Recovery-strain
λ and θ	Constants	τ_m	Torque of the motor
f_1	Frequency coincides with the first zero	R_p	The pitch radius of the pinion
f_2	Frequency coincides with the last pole	K	The meshing stiffness
σ	Stress	GMS	The gear mesh stiffness of the gear pair
ε	Strain	k_c	Contact stiffness
$\emptyset$	The phase angle	k_b	Bending stiffness
E'	Storage modulus	$\overline{I_i}$	Moment of inertia
E''	Loss modulus	$\overline{A_i}$	Area of the cross section
E_b	Bending modulus	S_i	Cross section
G	Shear modulus	n_s	Number of tooth slices
s_h	Shear factor	r	Radius of the tooth profile
n_b	Teeth number of the Nylon 6,6 gear	υ	Poisson's ratio
L_e	Length of a tooth		

2. The rheological model of the viscoelastic behaviour

Viscoelasticity is a combination of elastic and viscous behaviours. The elasticity of a material is an instantaneous behaviour and is often modelled using a linear spring (see **Fig. 1**(a)).

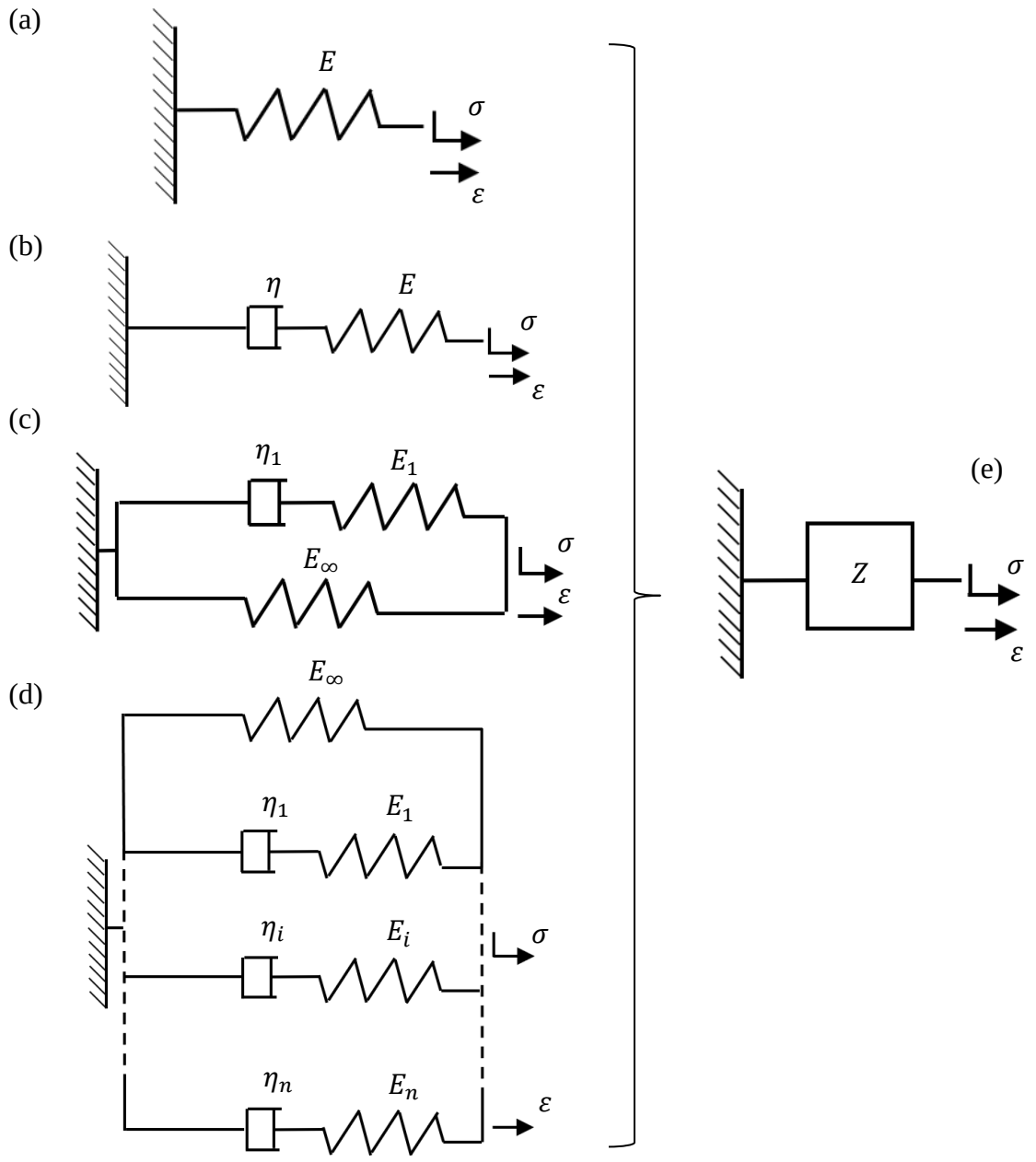

Fig. 1 (a) Linear spring, (b) Maxwell model (c) Zener model, (d) generalized Maxwell model and (e) the impedance of the corresponding model.

The impedance **Fig. 1**(e) of a spring is usually the Young's modulus of the material being modelled E, which is written as follows:

$$Z = E = \frac{\sigma}{\varepsilon} \tag{1}$$

Dashpots are added to springs to model the viscous behaviour. Usually, they are added to a spring in parallel or in series. When springs and dashpots are combined and defined by the right parameters, they can model several types of materials. There are simple models such as Kelvin-

Voigt, Maxwell and Zener (Hristov, 2019). Generalized models, such as GKV or GMM, provide a better approximation of reality than non-generalized models, with a larger number of parameters to be identified (Serra-Aguila et al., 2019). This study focuses on modelling the behaviour of a Nylon 6,6 gear meshed with a steel pinion. Therefore, GMM, a combination of Maxwell cells (i.e., Maxwell model) connected in parallel, is chosen. By adding a dashpot in series with a spring, the combination becomes a Maxwell model (see **Fig. 1**(b)). The inverse of the impedance in Maxwell's model is written in a complex form as follows, where ω is the angular frequency:

$$\frac{1}{Z(\omega)} = \frac{1}{E} + \frac{1}{j\omega\eta} \tag{2}$$

Therefore, the impedance becomes:

$$Z(\omega) = \frac{j\omega E\eta}{E + j\omega\eta} \tag{3}$$

When a Maxwell model is connected to a spring in parallel, it becomes a Zener model that is shown in **Fig. 1**(c) (i.e., GMM with only one Maxwell cell). The impedance of this model is then written as follows:

$$Z(\omega) = E_\infty + \frac{j\omega E_1\eta_1}{E_1 + j\omega\eta_1} \tag{4}$$

GMM consists of several Maxwell cells mounted in parallel as shown in **Fig. 1**(d). Each Maxwell cell is composed of a spring E_i and a dashpot η_i connected in series. Eventually, their combination in GMM can properly model the viscoelastic behaviour of polymers. A single spring E_∞ is also connected in parallel to the Maxwell cells to model the static stiffness. The rheological formulation of the impedance Z is written as follows:

$$Z(\omega) = E_\infty + \sum_{i=1}^{n} \frac{j\omega E_i\eta_i}{E_i + j\omega\eta_i} \tag{5}$$

Where $i \in [1\ n]$ and n is the number of Maxwell cells. With this model, it is possible to obtain different types of results. It is proposed to use it to investigate the creep-recovery of each tooth individually to eventually determine the GMS. In the study of Rosato et al. (Rosato et al., 2001), it is mentioned that the shape of strain depends on the type of stress applied. After considering a harmonic stress applied on a gear tooth, it is possible to have the strain-time curve which shows the said creep-recovery phenomenon. The proposed shape of this curve correlates with that given by the mentioned study.

3. Parameter identification method

It is mentioned in the study of Renaud et al. (Renaud et al., 2011) that PZF are very suitable for identifying parameters on transfer functions. It based on the CRONE method which is mentioned in the study by Oustaloup (A. Oustaloup, 1991). It takes the frequency domain and divides it into frequency sub-domains of equal length for each pole-zero couple. This method considers the area under the test curve and approaches it with an area of a rectangle with the height of the phase value

of the corresponding subdomain. Then, zeros are taken at random with the value equal to the first value of the subdomain while poles are deduced from zeroes. Then, a correction is made on the first zero $\omega_{z,1}$ and the last pole $\omega_{p,n}$ to eliminate the edge effects that appear in this method. The main drawback of this method is its unreliability for non-smooth phase curves, which is not the case in this study. The first zero and the last pole are identified directly from the experimental creep-strain curve. With CRONE approach, the sum of terms in equation (5) becomes a product which is given by equation (6) of the PZF.

$$Z(\omega) = E_\infty \prod_{i=1}^{n} \frac{1 + j\omega/\omega_{z,i}}{1 + j\omega/\omega_{p,i}} \tag{6}$$

Where, z and p are indices to identify a zero and a pole, respectively. Usually, the impedance $Z(\omega)$ (see equation (6)) of PZF is stress divided by strain. Therefore, it can be considered as a transfer function. Generally, the identification method uses the experimental data of modulus $|Z(\omega)|$ and phase $\emptyset(\omega)$ of the transfer function $Z(\omega)$ which can be written in the following expression:

$$Z(\omega) = |Z(\omega)| e^{(j\emptyset(\omega))} \tag{7}$$

The modulus $|Z(\omega)|$ and phase $\emptyset(\omega)$ of the associated PZF are written as follows (Renaud et al., 2011)):

$$|Z(\omega)| = E_\infty \prod_{i=1}^{n} \frac{\sqrt{1 + \left(\omega/\omega_{z,i}\right)^2}}{\sqrt{1 + \left(\omega/\omega_{p,i}\right)^2}} \tag{8}$$

$$\emptyset(\omega) = \sum_{i=1}^{N} \left(\tan^{-1}\left(\frac{\omega}{\omega_{z,i}}\right) - \tan^{-1}\left(\frac{\omega}{\omega_{p,i}}\right) \right) \tag{9}$$

In this study, the investigation focuses on gear teeth where the applied loads are harmonic. The frequency of these loads is low compared to the ones used in experimental Dynamic Mechanical Analysis (DMA) tests. The identification method is based on a creep-strain experimental measurement performed by Almagableh et al. (Almagableh et al., 2008). The test is done on a Nylon 6,6 specimen with dimensions of $18.5 \times 10 \times 1.6\text{mm}^3$. The attempt here is to use this creep-strain test and deduce poles and zeros to finally obtain the same curve numerically. The GMM parameters are thus deduced to eventually use them to model the behaviour of the Nylon 6,6 gear. **Fig. 2** shows the parameters that are directly identified from experiment (i.e., E_∞, $\omega_{z,1}$ and $\omega_{p,n}$).

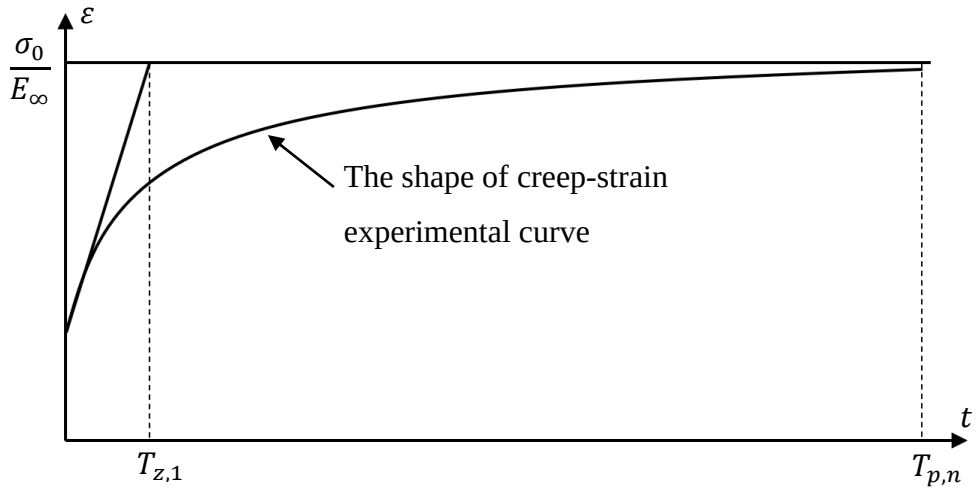

Fig. 2 Identified parameters from the experimental creep-strain curve.

The period of the first zero $T_{z,1}$ can be directly identified from the first asymptote at $t_0 = 0s$. The period of the last pole can be identified from the period of the experimental creep-strain test (i.e., at $t = T_{p,n}$). The static modulus $E_\infty$is identified from the asymptote of the last measured point. Using Zener model (Mainardi & Spada, 2011), the period of the first zero $T_{z,1}$ is deduced and written as follows:

$$T_{z,1} = \frac{\eta_1}{E_1} + \frac{\eta_1}{E_\infty} \tag{10}$$

The first zero and pole can be deduced from the impedance as follows (Renaud et al., 2011):

$$Z(\omega) = E_\infty + \frac{j\omega E_1 \eta_1}{E_1 + j\omega\eta_1} = E_\infty \frac{1 + j\omega\left(\frac{\eta_1}{E_1} + \frac{\eta_1}{E_\infty}\right)}{1 + j\omega\frac{\eta_1}{E_1}} = E_\infty \frac{1 + \frac{j\omega}{\omega_{z,1}}}{1 + \frac{j\omega}{\omega_{p,1}}} \tag{11}$$

$$\omega_{z,1} = \left(\frac{\eta_1}{E_1} + \frac{\eta_1}{E_\infty}\right)^{-1} = \frac{1}{T_{z,1}} = \frac{E_\infty E_1}{\eta_1(E_\infty + E_1)} \tag{12}$$

$$\omega_{p,1} = \left(\frac{\eta_1}{E_1}\right)^{-1} = \frac{E_1}{\eta_1} \tag{13}$$

The first zero and the last pole are sufficient to deduce the remaining poles and zeros. Therefore, the first pole is not used here. To achieve this, the constant phase approach mentioned in the work of Jrad et al. (Jrad et al., 2013) is used here. The phase angle between a pole and a zero is considered equal to $\frac{\pi}{2}$ when they are with the same order and equal to 0 elsewhere (see **Fig. 3**). This approach considers an estimated average phase angle of the impedance $Z(\omega)$ (see equations (6) and (7)). It is measured between the first zero and the last pole in the studied frequency range.

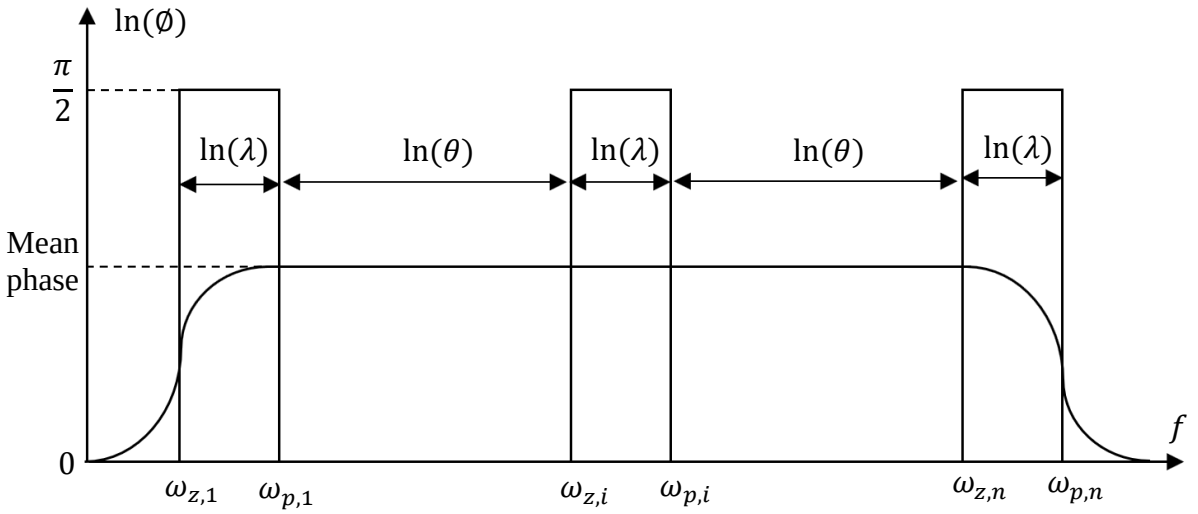

Fig. 3 Approach of constant phase.

The ratio between two consecutive poles is equal to the ratio between two consecutive zeros. This ratio must be constant to obtain a constant phase between two consecutive zeros. Two constants λ and θ are identified in equations (14) and (15):

$$\ln(\lambda) = \emptyset \frac{\ln(f_2) - \ln(f_1)}{\emptyset + \frac{\pi}{2}(n-1)} \tag{14}$$

$$\ln(\theta) = (\frac{\pi}{2} - \emptyset) \frac{\ln(f_2) - \ln(f_1)}{\emptyset + \frac{\pi}{2}(n-1)} \tag{15}$$

The average phase angle $\emptyset$ is identified in the frequency domain considered $[f_1\ f_2]$. The first zero and the last pole coincide with f_1 and f_2 respectively. Zeros are deduced from the first zero following equation (16):

$$\omega_{z,i+1} = \omega_{z,i} \lambda\ \theta \tag{16}$$

While poles are deduced from the last pole equation (17):

$$\omega_{p,i} = \frac{\omega_{p,i+1}}{\lambda\ \theta} \tag{17}$$

The constant λ is what relates poles and zeroes:

$$\omega_{p,i} = \lambda \omega_{z,i} \tag{18}$$

Eventually, parameters of GMM are deduced from the identified poles and zeros following these relations:

$$E_i = E_\infty \prod_{h=1}^{N} \left(\frac{\omega_{p,h}}{\omega_{z,h}}\right)\left(\frac{\omega_{p,i} - \omega_{z,h}}{\omega_{p,i} + \omega_{p,h}(\delta_{ih} - 1)}\right) \tag{19}$$

$$\eta_i = \frac{E_i}{\omega_{p,i}} \tag{20}$$

The procedure to find relations (19) and (20) is the linkage between PZF (equations (6) and (7)) and GMM parameters (equation (5)). It is detailed in the study of Renaud et al. (Renaud et al., 2011). The flow chart of the procedure to determine GMM parameters is shown in **Fig. 4**.

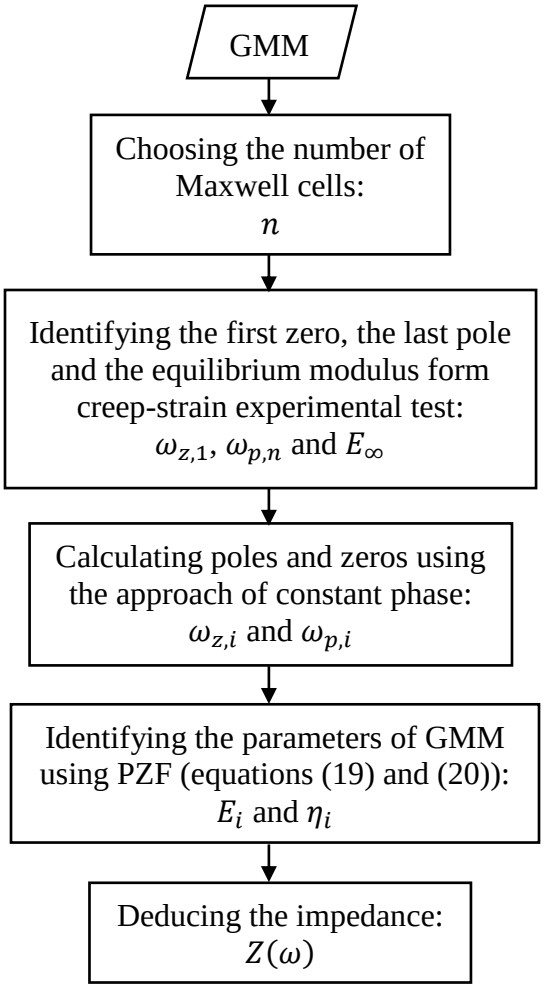

Fig. 4 Flow chart of GMM.

4. Numerical procedure

To properly model the results of a creep-strain test using GMM, it is suggested to use 5 Maxwell cells (i.e., n=5). This number is chosen by considering the minimum possible number of cells to model the results in the most adequate way. With a processor Intel(R) Core(TM) i5 and a memory card of 8Go RAM, the simulations with 5 Maxwell cells take 5 seconds to identify GMM parameters. With 4 Maxwell cells, the results are 10% less accurate than 5 Maxwell cells. With 6 Maxwell cells, however, the simulation time is 10 seconds, which is double the time of the chosen configuration with almost the same accuracy of 5 Maxwell cells (i.e., less than 1% more accurate). With more cells, the results are similar, but each added cell doubles the time needed. Therefore, the most appropriate number of cells is 5 for the proposed study. Yet, more cells can give similar results as well. The identified parameters of GMM using PZF are presented in **Table. 1**.

Table. 1 Parameters of GMM at 28°C

$E_\infty = 1300$ MPa	$\eta_1 = 1505$ N s/mm^2
$E_1 = 1626$ MPa	$\eta_2 = 2223$ N s/mm^2
$E_2 = 2801$ MPa	$\eta_3 = 2873$ N s/mm^2
$E_3 = 4222$ MPa	$\eta_4 = 3849$ N s/mm^2
$E_4 = 6600$ MPa	$\eta_5 = 7461$ N s/mm^2
$E_5 = 14923$ MPa	

In this paper, a simulation of the results of a creep-strain test, found by Almagableh et al. (Almagableh et al., 2008), is carried out. The parameters of GMM are chosen in the simulation process to properly model the results of the creep-strain test. This allows the creep-strain of pure Nylon 6,6 to be correctly modelled at different temperatures, as shown in **Fig. 5**.

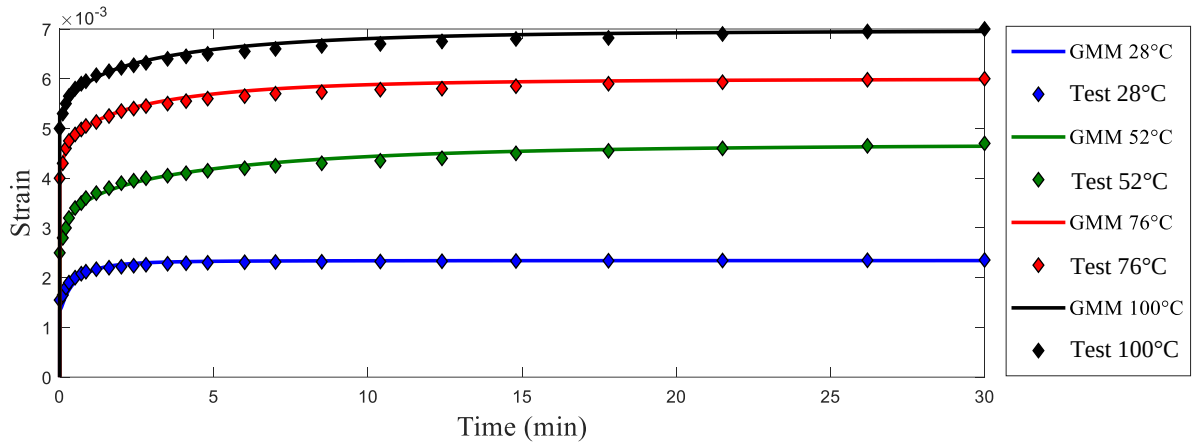

Fig. 5 Numerical and experimental data of creep-strain of Nylon 6,6 at 28°C, 52°C, 76°C and 100°C.

The numerical and experimental data show a good correlation. Therefore, the creep-recovery of Nylon 6,6 can be found in different geometries and different applied loads. The creep-strain response is based on the fact that equation (1) can be divided into the following form:

$$Z(\omega) = E'(\omega) + i\,\omega E''(\omega) \tag{21}$$

Where E' and E'' are the storage modulus and the loss modulus, respectively. Creep and recovery are deduced from the storage and the loss modulus, respectively. Therefore, creep-strain curve is determined from the following relation:

$$\varepsilon_{creep}(t) = \frac{\sigma}{E'} \tag{22}$$

While recovery-strain is determined using the following:

$$\varepsilon_{recovery}(t) = \frac{\sigma}{\omega E''} \tag{23}$$

Having correctly modelled the behaviour of Nylon 6,6, it is now possible to adapt it to find the GMS of the pair of gears proposed in this paper. Modelling the load sharing in metal gears can be

approximated easily with a load sharing factor. However, it is tricky when polymer gears are used. Many advanced load sharing models are proposed by different researchers (Melick, 2007)(Letzelter et al., 2011)(Cathelin et al., 2015). This study is considered an initiation to a new approach to model the GMS of a polymer-metal spur gear. It is therefore proposed to use an approximated model deduced from the one proposed in the study of Melick (Melick, 2007). The load sharing found by Melick is deduced by means of finite element analysis for different configurations of Stanyl gears (Stanyl GF30, Stanyl UF 23°C and Stanyl UF 140°C) coupled to a metal pinion. Stanyl is in fact the commercial name for Nylon 4,6 which is a material similar to Nylon 6,6 but with a higher modulus and melting point. The idea here is to derive an approximation of a load sharing model of Nylon 6.6 (with a modulus equal to 1300 MPa) by fitting the curve of the load sharing of Nylon 4.6 at 23°C (with a modulus equal to 3000 MPa) and Nylon 4.6 at 140°C (with a modulus equal to 700 MPa). An accurate load sharing model specific to the Nylon 6.6-metal gear pair can give more credibility to this work.

This approach considers a load-sharing function that takes into account the amount of load being shared between the engaged teeth. After contemplating this function, the stress can thus be obtained (see **Fig. 6)**. **Fig. 6**(a) shows the stress applied on one tooth for one cycle. **Fig. 6**(b) shows the details of load sharing between a tooth and the teeth in its vicinity. **Fig. 6**(c) shows the part of the tooth that are involved in the engagement, maintaining and disengagement periods.

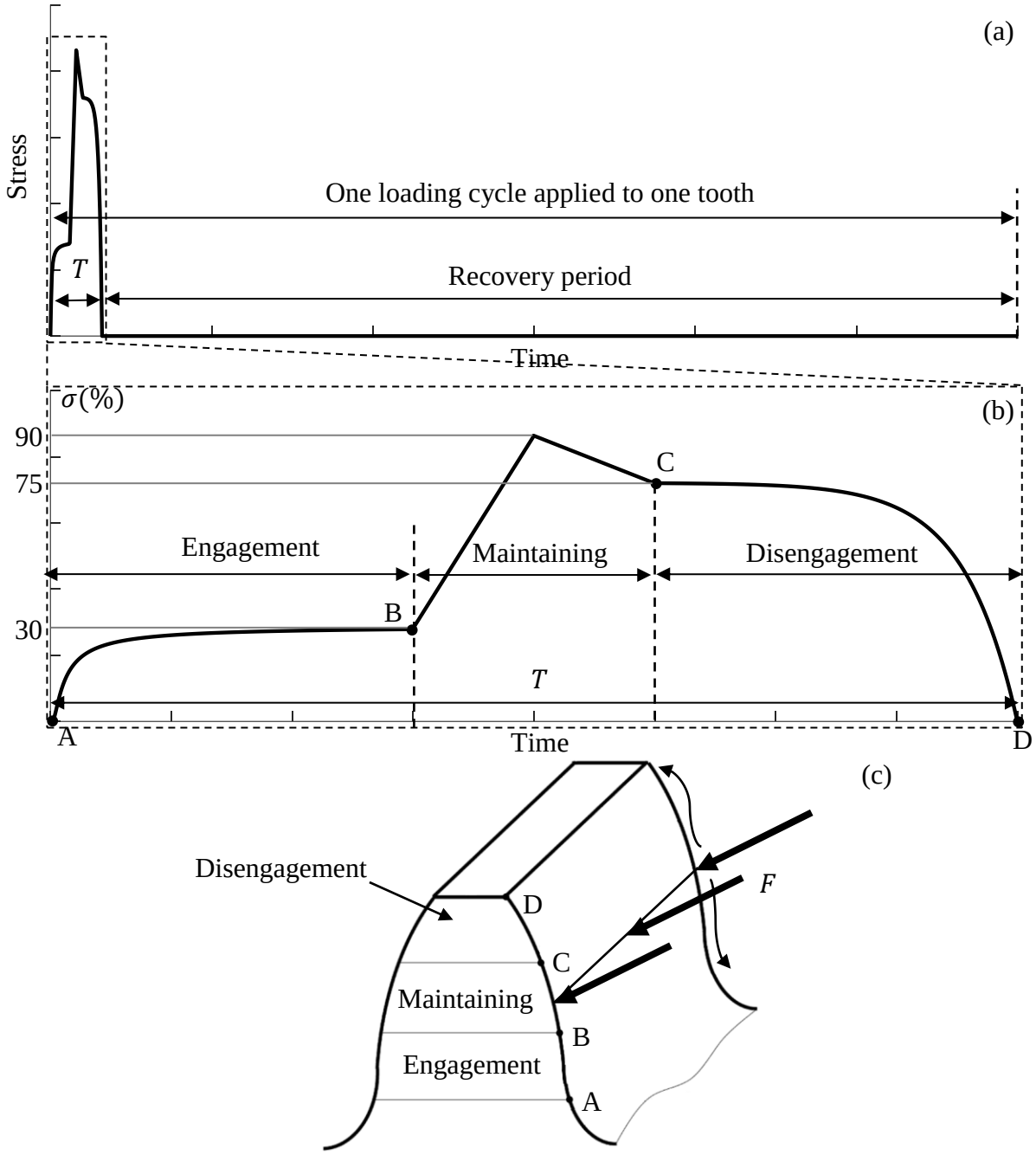

Fig. 6 (a) Shared stress in a single tooth cycle. (b) single tooth meshing period. (c) load distribution in the contact line between teeth.

The load applied to the gear teeth is measured from the torque applied to the supporting shaft. Each tooth is meshed during a period T from the engagement to the disengagement. For the engagement period, the load shared between teeth reach only 30% of the total load. In the maintaining period, the load shared reaches 90% of the applied load. Then, in the period of the disengagement, the load shared decreases from 75% of the total load to reach the last point of contact (see **Fig. 6**(b)).

After putting everything in place, it is now possible to proceed with numerical procedures to determine the GMS.

5. Numerical GMS of a polymer-metal spur gear system

The details of the gear pair used in this study are given in **Table. 2**.

Table. 2 Characteristics of the gear system

	Pinion	Gear
Teeth numbers	20	30
Material	Steel (S45C)	Pure Nylon 6,6
Base circle (mm)	18.8	28.2
Torque (N m)	24	-36
Rotation speed (rpm)	300	200
Radius of tooth profile (mm)	8	12
Poisson's ratio		0.38
Module (mm)	2	
Pressure angle α (°)	20	
Teeth width (mm)	23	
Contact ratio	c = 1.6	

It is shown in **Fig. 7** that GMM is used to model the behaviour of Nylon 6,6. In case of a polymer gear meshing with a steel pinion, Singh et al. (Singh et al., 2018) mentionned that the entire deformation will be on the polymer gear due to the low strength of the polymeric material. Therefore, it is assumed that the steel pinion will not be subject to deformation. The length of the contact line is equal to the face width of the teeth. The GMS $K(t)$ is deduced by considering engagement, maintaining and disengagement periods. The gearmesh period T_m is the sum of $(c-1)T_m$ during which the engagement or the disengagement is undergoing and $(2-c)T_m$ the maintaining period.

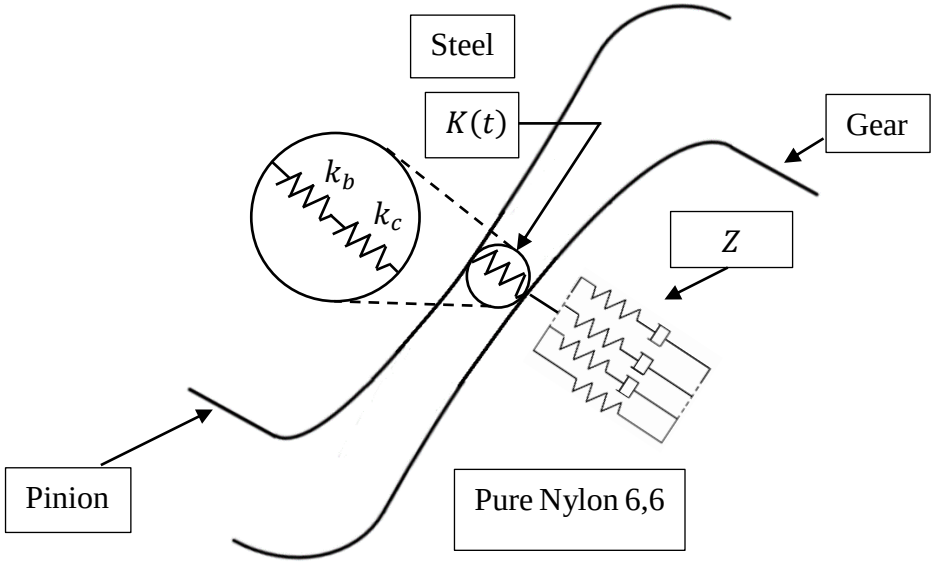

Fig. 7 The gear pair contact model.

The GMS $K(t)$ considered as two springs connected in series. The first one is used to model the bending stiffness k_b, and the other one is used to model the contact stiffness k_c. The teeth of the

spur gear exhibit minimum torsional deflection. Nevertheless, the torsional deflection of the drive shafts is not taken into account, as this requires a dynamic model with several degrees of freedom to be considered, which is beyond the scope of this manuscript. However, this deflection become more influential when different types of gears (e.g., helical or bevel …) are studied.

It is mentioned in the study of Melick (Melick, 2007) that polymer gears exhibit considerable bending, therefore the deflection due to this bending must be considered. It is assumed that a gear tooth can be modelled as a nonuniform cantilever beam (see **Fig. 8**).

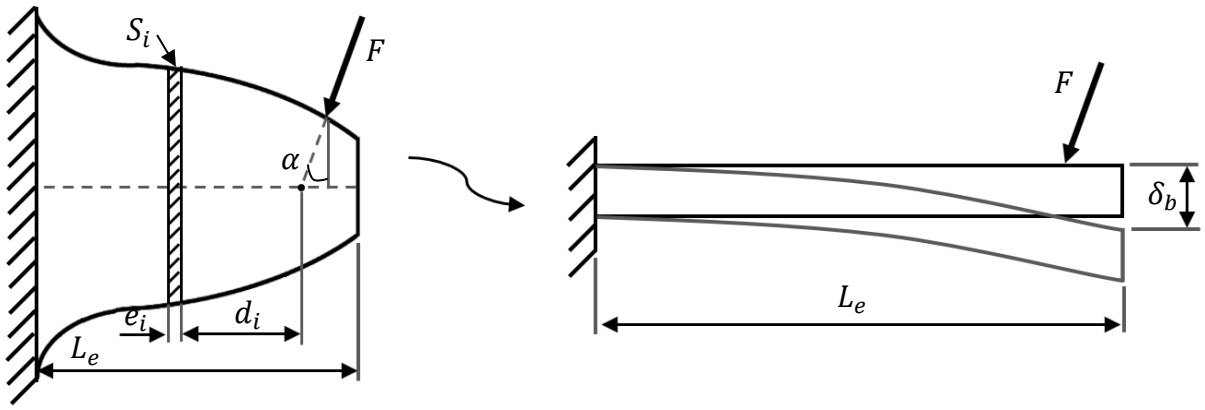

Fig. 8 The maximum bending deflection.

The bending deflection is measured as follows (Chaari et al., 2008):

$$\delta_b = F\cos^2\alpha \sum_{i=1}^{n_s} e_i \left(\frac{FL_e^3 d_i - e_i d_i + \frac{1}{3}e_i^2}{E_b \overline{I_\iota}} + \frac{1}{s_h G \overline{A_\iota}} + \frac{\tan^2\alpha}{E_b \overline{A_\iota}} \right) \tag{24}$$

L_e is the length of the tooth divided into n_s slices (see **Fig. 8**). The load applied by the metal pinion F, the pressure angle α, e_i and d_i are shown in **Fig. 8**. The moment of inertia $\overline{I_\iota}$ and the area $\overline{A_\iota}$ of the tooth cross sections S_i (see **Fig. 8**) are deduced using the following expressions:

$$\frac{1}{\overline{I_\iota}} = \left(\frac{1}{\overline{I_\iota}} + \frac{1}{\overline{I_{\iota+1}}} \right) / 2 \tag{25}$$

$$\frac{1}{\overline{A_\iota}} = \left(\frac{1}{\overline{A_\iota}} + \frac{1}{\overline{A_{\iota+1}}} \right) / 2 \tag{26}$$

The modulus E_b used to deduce the bending deflection is expressed as follows:

$$E_b = \frac{E_\infty (1-\upsilon)}{(1+\upsilon)(1-2\upsilon)} \tag{27}$$

Where υ and E_∞ are the Poisson's ration and the equilibrium modulus of the Nylon 6,6. Finally, the bending stiffness is expressed as follows:

$$k_b(t) = \frac{F}{\delta_b} \tag{28}$$

The contact deflection is considered to deduce the contact stiffness k_c (see equation (29)). Stiffness is the load divided by the deflection. In the proposed gear pair, it is equal to the load applied by the tangential load F_t (see equation (30)) divided by the contact deflection δ_c of the Nylon 6,6 gear.

$$k_c(t) = \frac{F_t}{\delta_c} \tag{29}$$

$$F_t = F\cos\alpha \tag{30}$$

Where F (see **Fig. 9**) is the load applied by the steel pinion deduced using the following:

$$F = \frac{\tau_m}{R_p} \tag{31}$$

Where τ_m and R_p are the torque applied to the shaft holding the pinion (e.g., the torque of a motor) and the pitch radius of the pinion, respectively.

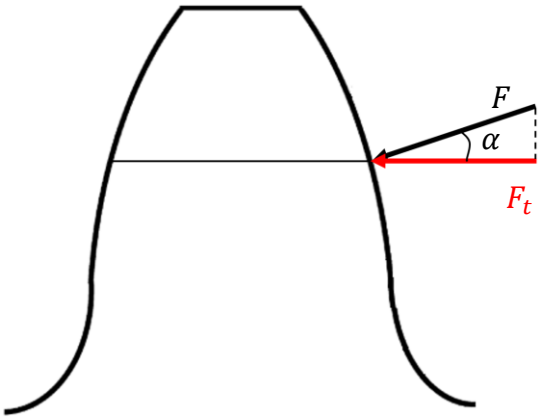

Fig. 9 Normal load.

α is the pressure angle and F_t is the tangential load applied by the metallic tooth. The distribution of tangential load F_t is shown in **Fig. 10**(a) and (b).

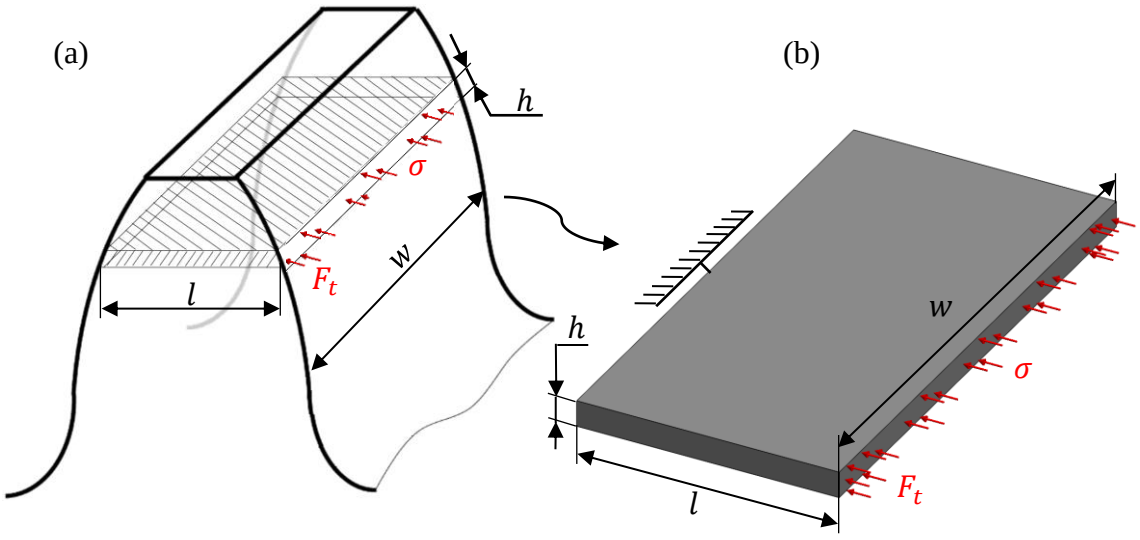

Fig. 10 Geometrical parameters involved in the contact stiffness determination in the tooth (a) being approximated as a beam (b).

The impedance Z is assumed to follow equation (32) where σ is the stress and ε is the strain:

$$Z(\omega) = \frac{\sigma}{\varepsilon(t)} \tag{32}$$

The load F_t is distributed as stress σ at a considered contact section. Stress is written as follows:

$$\sigma = \frac{F_t}{S} \tag{33}$$

With: $$S = wh \tag{34}$$

Where, w and h are respectively the face width of the tooth and the thickness of teeth contact. The latter is considered constant to simplify measurement. It is approximated using the Hertzian contact formula taking into account that all deformations will occur on the polymer gear. Therefore, the thickness of teeth contact is written as follows:

$$h = \sqrt{\frac{2F_t}{\pi w}\left(\frac{1-\upsilon^2/E_\infty}{1/2r}\right)} \tag{35}$$

Where r is the radius of the tooth profile of a gear presented in **Fig. 11**.

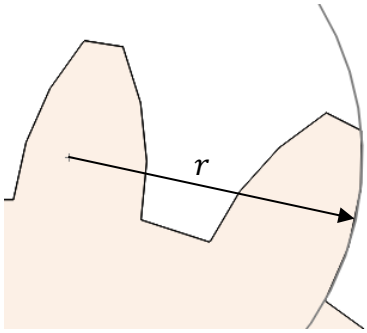

Fig. 11 radius of tooth profile

The deflection is considered as contraction divided by the initial length of a beam (see **Fig. 10**(b)). In this case, the contraction corresponds to the deflection resulted from teeth engagement and the initial length correspond to the initial thickness l of the tooth. Thus, the contact deflection can be expressed as follows:

$$\delta_c = l\varepsilon_{creep}(t) \tag{36}$$

The expression of creep-strain ε_{creep} is presented in equation (22). The variation of the chordal thickness of a tooth l is approximated directly from a linear variation between the dedendum and the addendum of a tooth. Finally, the single tooth meshing stiffness is deduced from equations (29), (33), (34) and (36) as:

$$k_c(t) = \frac{wh\sigma}{l\varepsilon_{creep}} \tag{37}$$

Creep-strain ε_{creep} expression is used directly from equation (22), it is not replaced here to keep the meshing stiffness expression in the time domain. Recovery-strain $\varepsilon_{recovery}$ is not introduced in the measurement of the single tooth meshing stiffness, because, in the period when teeth are not involved in the meshing, they do not influence the gear meshing. On the other hand, recovery of a tooth in a gear pair may not be total. It is therefore considered in subsequent revolutions of the gears taking into account the unrecovered deformation received by the teeth. Thus, recovery-strain will influence creep-strain that is influencing the GMS. Finally, the meshing stiffness of a single tooth is written as follows:

$$K(t) = 1/\left(\frac{1}{k_b} + \frac{1}{k_c}\right) \tag{38}$$

The stress $\sigma(t)$ is introduced by following the load sharing procedure shown in **Fig. 6**. The creep-recovery of a tooth over time is given in **Fig. 12**(a) at 28°C over time of multiple running cycles. A single running cycle is shown in **Fig. 12**(b) to visualize creep and recovery periods. Each tooth has a period of time $T = cT_m$ between engagement and disengagement of the gear. Creep is lasting along the period T. The non-linear forms represent the viscoelastic behaviour (see **Fig. 12**(c)). After that, the material tends to return to its initial state. Hence, the recovery phenomenon starts to

appear and lasts until the second engagement starts (see **Fig. 12**(c)) to reach a minimum value of strain of non-recovered material e.

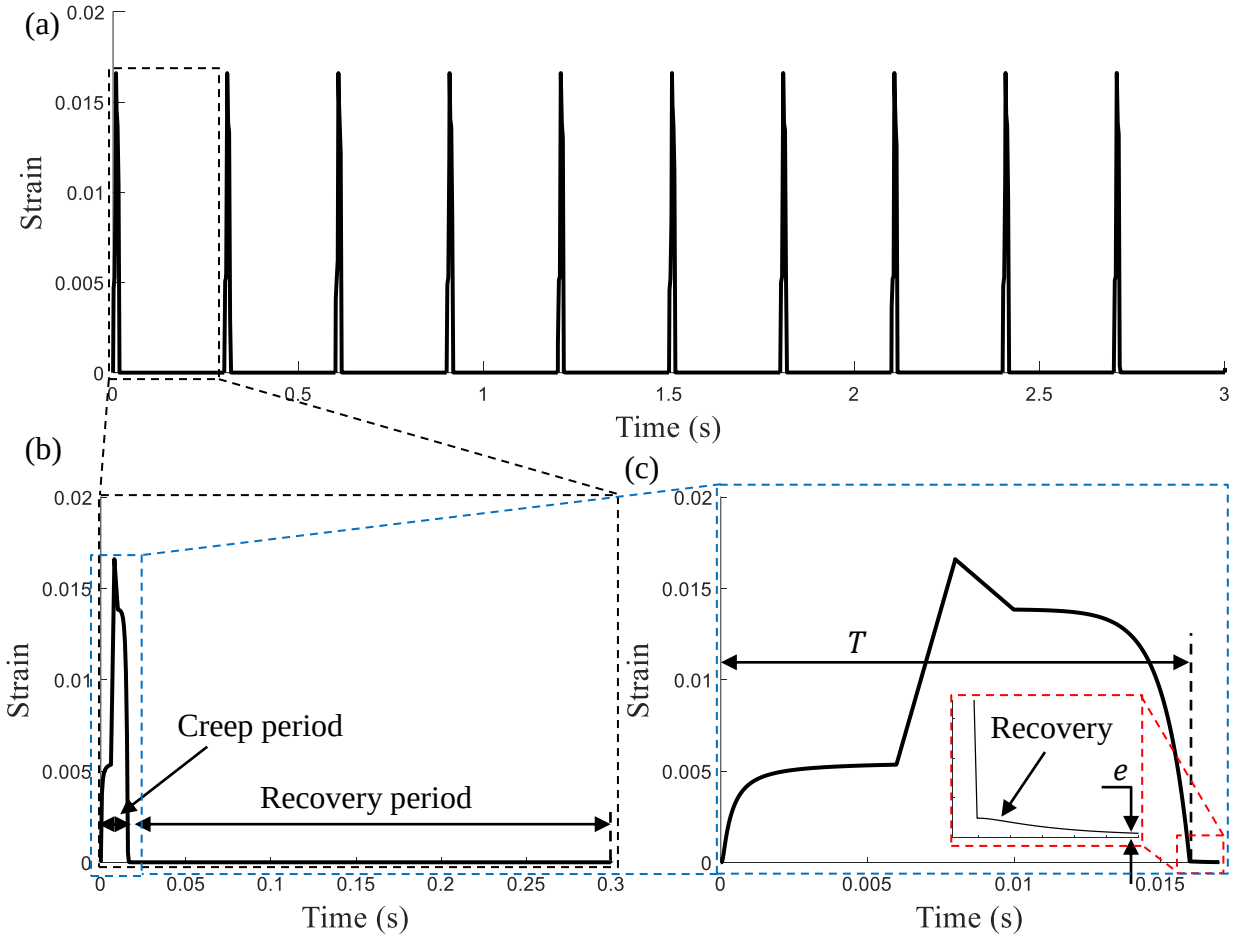

Fig. 12 (a) Creep-recovery of a gear tooth over time of multiple running cycles, (b) a single revolution and (c) a meshing period.

Upon loading period, the strain of a tooth is following a similar shape to the curve of the applied stress (see **Fig. 12**(c)). Afterwards, the tooth disengages and start a recovery phenomenon. It is mentioned in the study of Lunn et al. (Lunn et al., 1974) that Nylon 6,6 reaches not more than 85% of recovery after 100 sec at ambient temperature. Recovery is not total for this modelling because the time that takes the tooth to recover before the second engagement is less than 100 sec and not enough for full recovery. For these reasons, strain reaches a value of non-recovered material equal to e instead of zero for the first cycle (see **Fig. 12**(c)). Then, in each period, this value is added to the strain for each cycle as shown in **Fig. 12**(a). The stiffness of one tooth is deduced in a previous study (Chakroun et al., 2022b). The procedure followed is detailed in the flowchart **Fig. 13**.

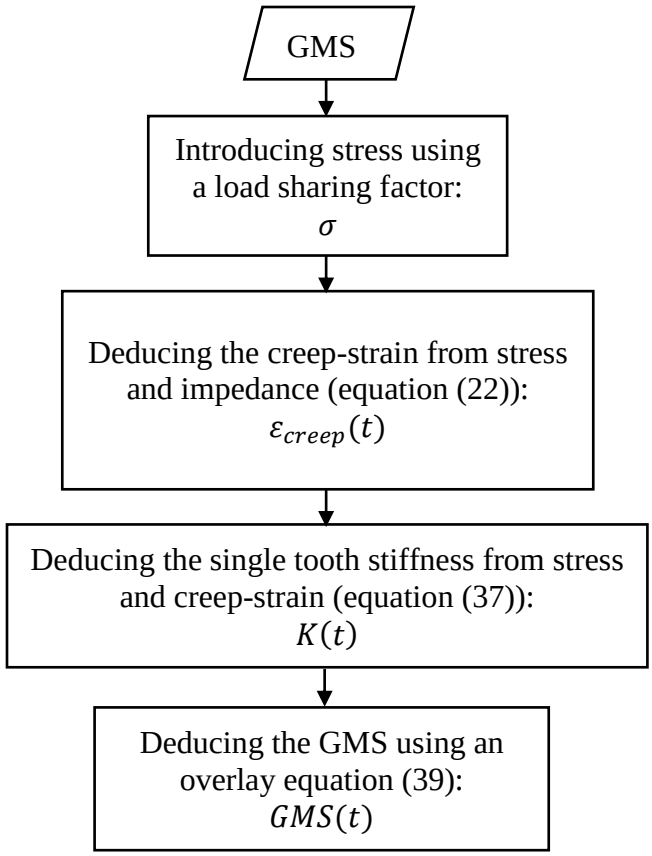

Fig. 13 Flow chart to deduce the GMS of a polymer-metallic spur gear system

The evolution of this stiffness over time is deduced following equation (37) and shown in **Fig. 14**.

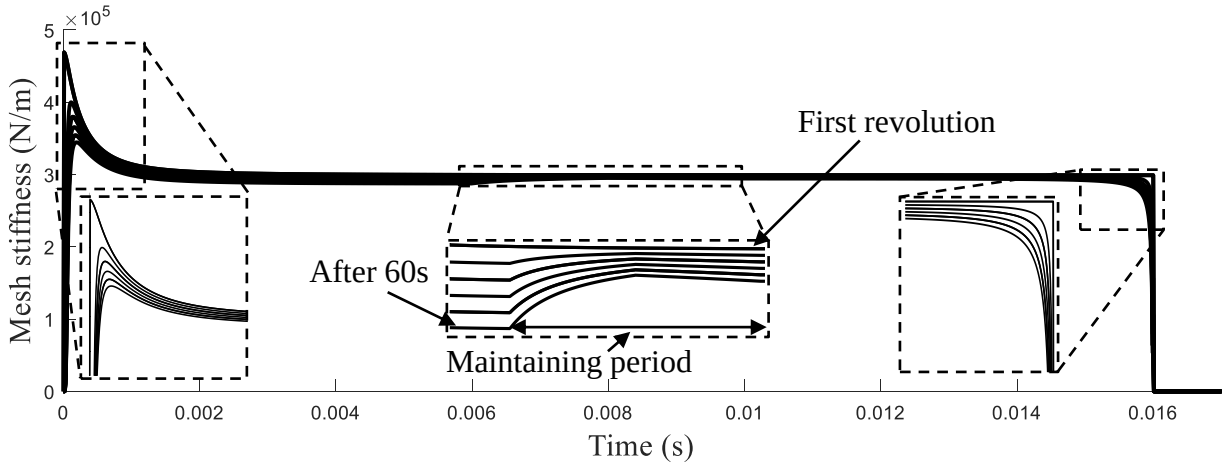

Fig. 14 Stiffness over time of one gear tooth.

The stiffness is presented in this figure for every 10s of functioning time. The behaviour of the stiffness in changing from an engagement period to another. This is due to the variation of the modulus of the material over time, as it is receiving a harmonic load. Initially, there is a delay in reaching a stationary stiffness. This is due to the viscous character of the viscoelastic material. After a period of operation, there is always a delay in the meshing stiffness signal. But the stiffness no longer reaches a steady state. It is influenced by previous engagements and each time the

material becomes softer than before. This results in a loss of stiffness and curved shapes. Also, the intermediate stage that appears in the stiffness of the engagement is the result high value of stress achieved in the maintaining period. Therefore, the contact portion of the maintaining period is influenced by the stress peak introduced between B and C, as shown in **Fig. 6**.

Having considered the behaviour of one tooth, it is now possible to deduce the behaviour of all the teeth in the gear system. The phase between two teeth is considered and applied for all teeth of the gear. From these stiffness signals, a superposition is followed to deduce the GMS of the gear pair. It is measured using the following:

$$GMS(t) = \sum_{i=1}^{n_b} K_i \tag{39}$$

Where n_b is the Nylon 6,6 gear teeth number and K_i is the stiffness of the corresponding tooth (deduced from equation (37)). The evolution of this overlay and the change in the shape of the GMS is shown in **Fig. 15**.

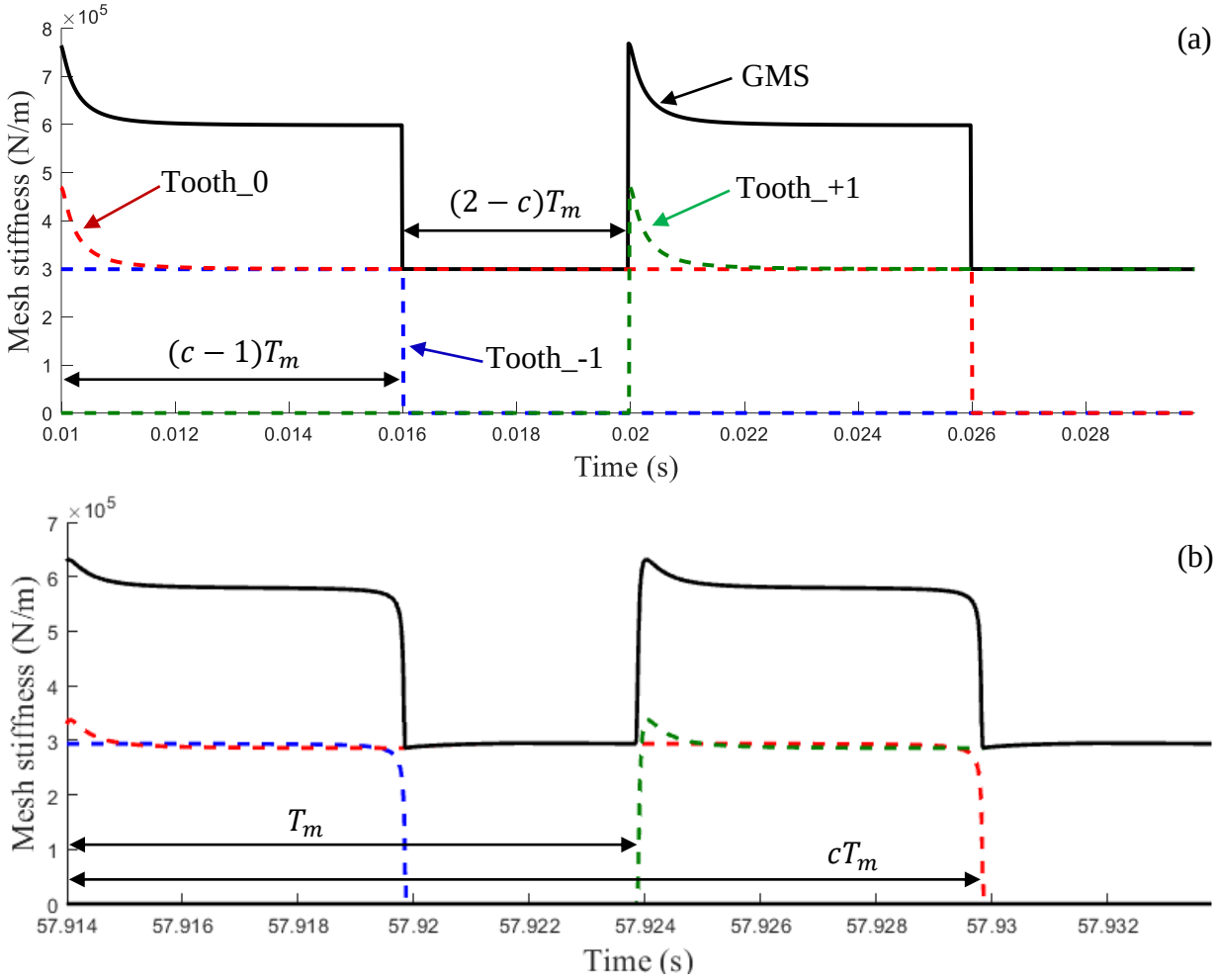

Fig. 15 : (a) The overlay done to deduce the GMS at the first engagement and (b) after 60s.

In the first revolution of the gear (see **Fig. 15**(a)), it can be seen that the GMS in the period of engagement (i.e., $(c-1)T_m$) behaving in the same way as for Tooth_0 with just adding the constant stiffness of Tooth_-1. In the period of maintaining (i.e., $(2-c)T_m$), the behaviour of the GMS is the same as that of the Tooth_0. After a running time (see **Fig. 15**(b)), the small change in the shape of the GMS over time is the result of the change of the shape of the single tooth meshing stiffness over time shown previously in **Fig. 14**. This small change can be significant for a much longer running time. Finally, the evolution of the GMS is shown in **Fig. 16**.

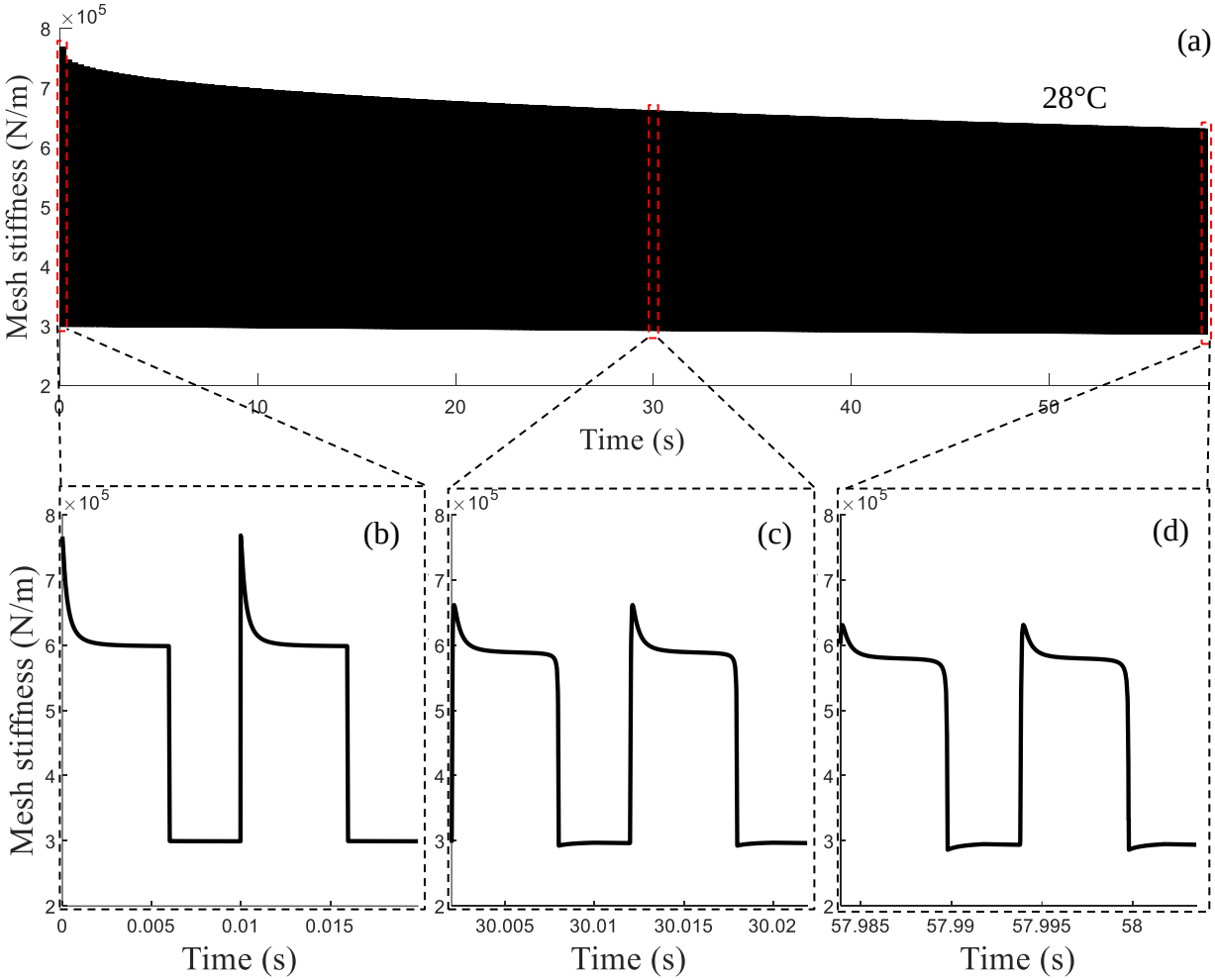

Fig. 16 : Evolution of GMS of the gear system by time (a) with a zoom in the beginning (b) in the middle (c) and the end (d) of the simulation.

Unlike metallic gears, the GMS cannot be modelled as a square signal that is usually used in metallic gear application. It is completely different when a polymer gear is used. It is also different from that found in a quasi-static study in which the behaviour does not progress with time (Chakroun et al., 2022a). Similarities are only noticed in the first revolution of the gear. The variation of GMS here is no longer periodic. It shows a decrease in both maximum and minimum values over time as shown in **Fig. 16**(a). This is because the recovery of Nylon 6,6 is not total each cycle. It is also the result of the material softening found in the single tooth stiffness presented in **Fig. 14**. In addition, it shows a change in the shape each meshing period, as shown in the zoom in **Fig. 16**(b), (c) and (d). It is clear that this shape is becoming more and more concave. Thus, this is

also the result of the non-total recovery. It is expected to show more visible changes for longer running time.

After investigating the influence of viscoelastic behaviour of Nylon 6,6 on the GMS of the studied gear pair, it is now proposed to study the influence of temperature. The simulated strain signals shown in **Fig. 5** at 28°C, 52°C, 76°C and 100°C are considered and the GMS is deduced and plotted in **Fig 17**.

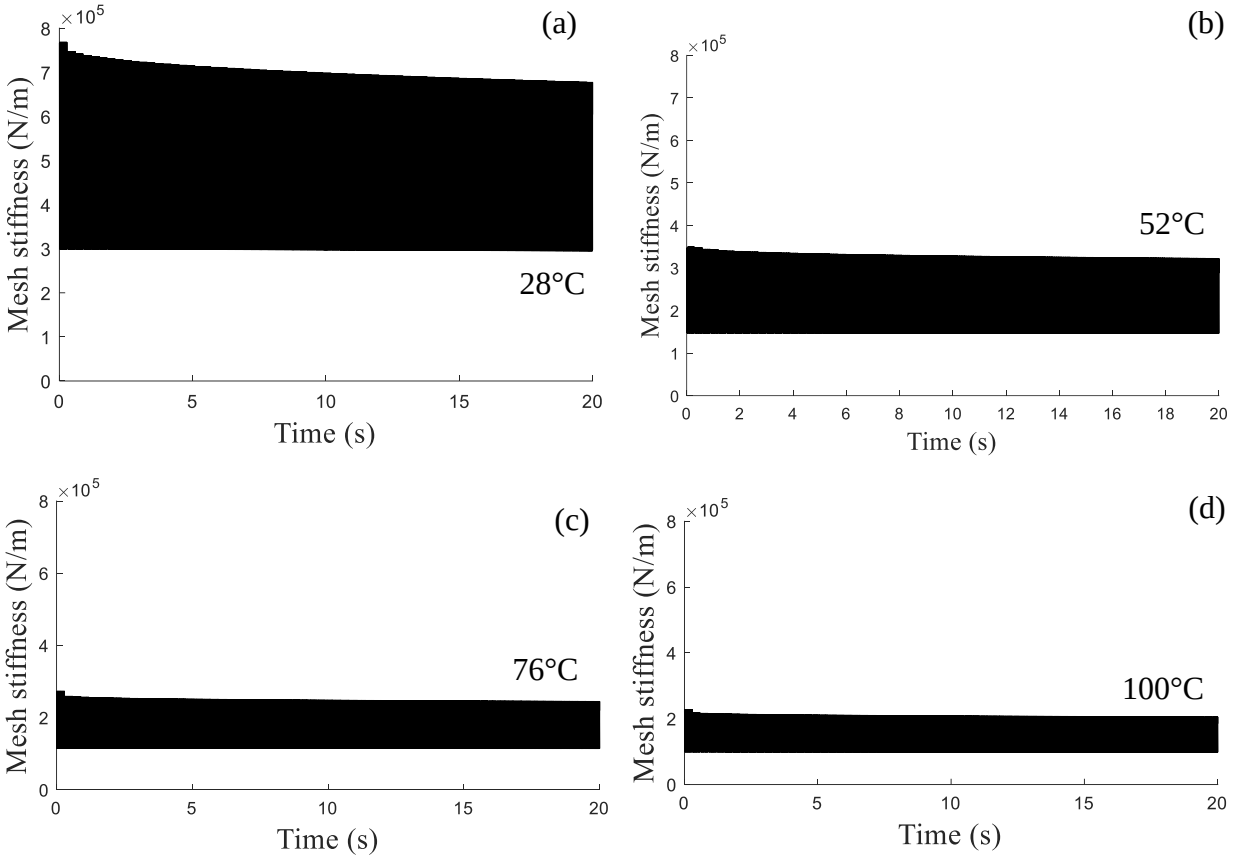

Fig 17 : Evolution of GMS of the gear system by time at 28°C (a), 52°C (b), 76°C (c) and 100°C (d)

It is known that polymers are very sensitive to temperature especially when compared to metal. Therefore, this fact can be clearly seen in **Fig 17**(a) and **Fig 17**(b) where a slight increase in temperature form 28°C to 52°C led to a major change in the GMS signal. In fact, this increase in temperature brought it close to the glass transition of Nylon 6,6 which is equal to 57°C according to Tobolsky method (Champetier & Pied, 1961) and equal to 58°C according to a differential thermal analysis (Greco & Nicolais, 1976). The maximum and minimum values are decreased to almost the half. In the other hand, the decrees over time become less steep. When more temperature is applied (see **Fig 17**(c) and **Fig 17**(d)), the change became less apparent.

6. Conclusion

Through this paper, a new approach of determining the gear mesh stiffness is presented. It uses generalized Maxwell model to simulate viscoelastic behaviour of Nylon 6,6 in gear applications. This approach brings together rheology with the study of gears. The results of the numerical

simulation illustrate that gear mesh stiffness maximum and minimum values decrease over time with a change in the shape of the signal. This is because the polymer gear teeth do not have enough time to recover from the deformation they undergo with each cycle. This is also the result of the softening effect of the material over running time. Finally, the gear mesh stiffness signal established in this study can be taken into consideration to investigate efficiently the dynamic behaviour and vibration responses of polymer-metallic spur gear systems. In addition, the non-total recovery and alternating tooth geometry lead to a time-varying load sharing. This variation will directly influence the GMS signal. This can lead to an interesting topic that faces a coupled problem. Therefore, a more advanced load sharing function that takes into account the change in shape of the gear teeth can provide an interesting addition to this study.

Acknowledgements

The authors would like to acknowledge Project DPI2017-85390-P funded by the Spanish Ministry of Economy, Industry, and Competitiveness for supporting this research. Moreover, the authors acknowledge the Projects PID2020-116213RB-I00 and PID2020-116572RA-I00 funded by the Spanish Ministry of Science and Innovation.

References

A. Oustaloup. (1991). *La commande CRONE: commande robuste d ' ordre non entier.* Hermes Science Publications.

Almagableh, A., Gupta, S., Mantena, P. R., & Al-Ostaz, A. (2008). Dynamic mechanical analysis of graphite platelet and nanoclay reinforced vinyl ester, and MWCNT reinforced nylon 6,6 nanocomposites. *International SAMPE Technical Conference*, *June*.

Bagley, R. L., & Torvik, P. J. (1985). Fractional calculus in the transient analysis of viscoelastically damped structures. *AIAA Journal*, *23*(6), 918–925. https://doi.org/10.2514/3.9007

Blanc, R. H., & Ravasoo, A. (1996). On the nonlinear viscoelastic behaviour of nylon fiber. *Mechanics of Materials*. https://doi.org/10.1016/0167-6636(95)00045-3

Cathelin, J., Guingand, M., de Vaujany, J. P., Chazeau, L., & Adrien, J. (2015). Quasi-static Load Sharing Model in the Case of Moulded Glass Fibre Reinforced Polyamide 6 Gears. *Applied Composite Materials*, *22*(4), 343–362. https://doi.org/10.1007/s10443-014-9410-7

Chaari, F., Baccar, W., Abbes, M. S., & Haddar, M. (2008). Effect of spalling or tooth breakage on gearmesh stiffness and dynamic response of a one-stage spur gear transmission. *European Journal of Mechanics, A/Solids*, *27*(4), 691–705. https://doi.org/10.1016/j.euromechsol.2007.11.005

Chaari, F., Fakhfakh, T., & Haddar, M. (2009). Analytical modelling of spur gear tooth crack and influence on gearmesh stiffness. *European Journal of Mechanics, A/Solids*, *28*(3), 461–468. https://doi.org/10.1016/j.euromechsol.2008.07.007

Chakroun, A. E., Hammami, A., De-Juan, A., Chaari, F., Fernandez, A., Viadero, F., & Haddar, M. (2021). Modal energetic analysis and dynamic response of worm gear drives with a new developed dynamic model. *Comptes Rendus. Mécanique*, *349*(2), 241–258. https://doi.org/10.5802/crmeca.80

Chakroun, A. E., Hammami, C., Hammami, A., De-Juan, A., Chaari, F., Fernandez, A., Viadero,

F., & Haddar, M. (2022a). Quasi-static Study of Gear Mesh Stiffness of a Polymer-Metallic Spur Gear System. In *Lecture Notes in Mechanical Engineering* (Vol. 2, pp. 301–307). https://doi.org/10.1007/978-3-030-84958-0_32

Chakroun, A. E., Hammami, C., Hammami, A., De-Juan, A., Chaari, F., Fernandez, A., Viadero, F., & Haddar, M. (2022b). Study of the Stiffness of a Polymer Pinion Tooth in a Polymer-Metallic Spur Gear System. In *Modelling and Simulation of Complex Systems for Sustainable Energy Efficiency* (Vol. 2, pp. 123–130). https://doi.org/10.1007/978-3-030-85584-0_13

Champetier, P. G., & Pied, J. P. (1961). Sur quelques propriétés physiques des polyamides. *Die Makromolekulare Chemie*, *44*(1), 64–70. https://doi.org/10.1002/macp.1961.020440106

Cui, L., Liu, T., Huang, J., & Wang, H. (2019). Improvement on meshing stiffness algorithms of gear with peeling. *Symmetry*, *11*(5), 1–14. https://doi.org/10.3390/sym11050609

de Vaujany, J.-P., Guingand, M., & Remond, D. (2008). Numerical and Experimental Study of the Loaded Transmission Error of a Worm Gear With a Plastic Wheel. *Journal of Mechanical Design*, *130*(6), 062602. https://doi.org/10.1115/1.2898877

Driss, Y., Ahmed, H., Lassaad, W., & Mohamed, H. (2014). Effects of gear mesh fluctuation and defaults on the dynamic behavior of two-stage straight bevel system. *Mechanism and Machine Theory*, *82*, 71–86. https://doi.org/10.1016/j.mechmachtheory.2014.07.013

Düzcükoğlu, H., Yakut, R., & Uysal, E. (2010). The use of cooling holes to decrease the amount of thermal damage on a plastic gear tooth. In *Journal of Failure Analysis and Prevention*. https://doi.org/10.1007/s11668-010-9398-8

Farhat, M. H., Hentati, T., Chiementin, X., Bolaers, F., Chaari, F., & Haddar, M. (2020). Numerical model of a single stage gearbox under variable regime. *Mechanics Based Design of Structurs and Machines*, *50*. https://doi.org/10.1080/15397734.2020.1863226

Fernandez Del Rincon, A., Viadero, F., Iglesias, M., García, P., De-Juan, A., & Sancibrian, R. (2013). A model for the study of meshing stiffness in spur gear transmissions. *Mechanism and Machine Theory*, *61*, 30–58. https://doi.org/10.1016/j.mechmachtheory.2012.10.008

Ganeriwala, S. N., & Rotz, C. A. (1985). Fourier Transform Mechanical Analysis Technique for Determining Non-Linear Dynamic Viscoelastic Behavior of Polymers. *American Chemical Society, Polymer Preprints, Division of Polymer Chemistry*, *26*(2), 164–165.

Greco, R., & Nicolais, L. (1976). Glass transition temperature in nylons. *Polymer*, *17*(12), 1049–1053. https://doi.org/10.1016/0032-3861(76)90005-7

Han, L., & Qi, H. (2019). Dynamic response analysis of helical gear pair considering the interaction between friction and mesh stiffness. *Meccanica*, *54*(15), 2325–2337. https://doi.org/10.1007/s11012-019-01088-y

Hasl, C., Liu, H., Oster, P., Tobie, T., Stahl, K., & Forschungsstelle fuer Zahnraeder und Getriebebau (Gear Research Centre). (2017). Method for calculating the tooth root stress of plastic spur gears meshing with steel gears under consideration of deflection-induced load sharing. *Mechanism and Machine Theory*, *111*, 152–163. https://doi.org/10.1016/j.mechmachtheory.2017.01.015

Henriot, G. (1985). *Traité théorique et pratique des engrenages, tome 1 et 2*. Edition Dunod

technique.

Hiltcher, Y., Guingand, M., & de Vaujany, J.-P. (2006). Load Sharing of Worm Gear With a Plastic Wheel. *Journal of Mechanical Design*, *129*(1), 23. https://doi.org/10.1115/1.2359469

Hristov, J. (2019). Linear viscoelastic responses and constitutive equations in terms of fractional operators with non-singular kernels: Pragmatic approach, memory kernel correspondence requirement and analyses. *European Physical Journal Plus*, *134*(6). https://doi.org/10.1140/epjp/i2019-12697-7

Imrek, H. (2009). Performance improvement method for Nylon 6 spur gears. *Tribology International*, *42*(3), 503–510. https://doi.org/10.1016/j.triboint.2008.08.011

Joo, W., Jepsen, K. J., & Davy, D. T. (2007). The effect of recovery time and test conditions on viscoelastic measures of tensile damage in cortical bone. *Journal of Biomechanics*, *40*(12), 2731–2737. https://doi.org/10.1016/j.jbiomech.2007.01.005

Jrad, H., Dion, J. L., Renaud, F., Tawfiq, I., & Haddar, M. (2013). Experimental characterization, modeling and parametric identification of the non linear dynamic behavior of viscoelastic components. *European Journal of Mechanics, A/Solids*, *42*, 176–187. https://doi.org/10.1016/j.euromechsol.2013.05.004

Jrad, H., Dion, J. L., Renaud, F., Tawfiq, I., & Haddar, M. (2017). Experimental and numerical investigation of energy dissipation in elastomeric rotational joint under harmonic loading. *Mechanics of Time-Dependent Materials*, *21*(2), 177–198. https://doi.org/10.1007/s11043-016-9325-9

Kim, C. H. (2006). Durability improvement method for plastic spur gears. *Tribology International*. https://doi.org/10.1016/j.triboint.2006.01.020

Kodeeswaran, M., Suresh, R., & Senthilvelan, S. (2017). Effect of strain rate on bending and transmission characteristics of injection molded polyamide 66 spur gears. *Proceedings of the Institution of Mechanical Engineers, Part L: Journal of Materials: Design and Applications*, *0*(0), 146442071772448. https://doi.org/10.1177/1464420717724484

Letzelter, E., de Vaujany, J. P., & Guingand, M. (2011). Load-sharing model for polymer cylindrical gears. *Gear Technology*, 28–34. (hal-00689480)

Li, W., Wood, A., Weidig, R., & Mao, K. (2011). An investigation on the wear behaviour of dissimilar polymer gear engagements. *Wear*. https://doi.org/10.1016/j.wear.2010.11.019

Lin, A. Der, & Kuang, J. H. (2008). Dynamic interaction between contact loads and tooth wear of engaged plastic gear pairs. *International Journal of Mechanical Sciences*, *50*(2), 205–213. https://doi.org/10.1016/j.ijmecsci.2007.07.002

Lunn, A. C., Lee, B. -L, & Yannas, I. V. (1974). Strain recovery of polyester and nylon 66 monofilaments under various temperature histories. *Polymer Engineering & Science*, *14*(9), 610–615. https://doi.org/10.1002/pen.760140904

Mainardi, F., & Spada, G. (2011). Creep, relaxation and viscosity properties for basic fractional models in rheology. *European Physical Journal: Special Topics*, *193*(1), 133–160. https://doi.org/10.1140/epjst/e2011-01387-1

Mao, K., Li, W., Hooke, C. J., & Walton, D. (2009). Friction and wear behaviour of acetal and nylon gears. *Wear*. https://doi.org/10.1016/j.wear.2008.10.005

Marafona, J. D. M., Marques, P. M. T., Martins, R. C., & Seabra, J. H. O. (2021). Mesh stiffness models for cylindrical gears: A detailed review. *Mechanism and Machine Theory*, *166*(July), 104472. https://doi.org/10.1016/j.mechmachtheory.2021.104472

Melick, D. I. H. G. H. van. (2007). Tooth-Bending Effects in Plastic Spur Gears. *Gear Technology*.

Mertens, A. J., & Senthilvelan, S. (2016). Durability of polymer gear-paired with steel gear manufactured by wire cut electric discharge machining and hobbing. *International Journal of Precision Engineering and Manufacturing*. https://doi.org/10.1007/s12541-016-0023-y

Meuleman, P. K., Walton, D., Dearn, K. D., Weale, D. J., & Driessen, I. (2007). Minimization of transmission errors in highly loaded plastic gear trains. *Proceedings of the Institution of Mechanical Engineers, Part C: Journal of Mechanical Engineering Science*. https://doi.org/10.1243/09544062JMES439

Renaud, F., Dion, J. L., Chevallier, G., Tawfiq, I., & Lemaire, R. (2011). A new identification method of viscoelastic behavior: Application to the generalized Maxwell model. *Mechanical Systems and Signal Processing*. https://doi.org/10.1016/j.ymssp.2010.09.002

Rosato, D. V., Rosato, D. V., & Rosato, M. G. (2001). *Plastics Design Handbook*. Springer US. https://doi.org/10.1007/978-1-4615-1399-5

Serra-Aguila, A., Puigoriol-Forcada, J. M., Reyes, G., & Menacho, J. (2019). Viscoelastic models revisited: characteristics and interconversion formulas for generalized Kelvin–Voigt and Maxwell models. *Acta Mechanica Sinica/Lixue Xuebao*, *35*(6), 1191–1209. https://doi.org/10.1007/s10409-019-00895-6

Shen, J., Hu, N., Zhang, L., & Luo, P. (2020). Dynamic analysis of planetary gear with root crack in sun gear based on improved time-varying mesh stiffness. *Applied Sciences (Switzerland)*, *10*(23), 1–20. https://doi.org/10.3390/app10238379

Singh, A. K., Siddhartha, & Singh, P. K. (2018). Polymer spur gears behaviors under different loading conditions: A review. *Proceedings of the Institution of Mechanical Engineers, Part J: Journal of Engineering Tribology*, *232*(2), 210–228. https://doi.org/10.1177/1350650117711595

Sun, X., Zhao, Y., Liu, M., & Liu, Y. (2019). On Dynamic Mesh Force Evaluation of Spiral Bevel Gears. *Shock and Vibration*, *2019*. https://doi.org/10.1155/2019/5614574

Tsai, M. H., & Tsai, Y. C. (1997). A method for calculating static transmission errors of plastic spur gears using FEM evaluation. *Finite Elements in Analysis and Design*, *27*(4), 345–357. https://doi.org/10.1016/S0168-874X(97)81968-3

Walha, L., Driss, Y., Khabou, M. T., Fakhfakh, T., & Haddar, M. (2011). Effects of eccentricity defect on the nonlinear dynamic behavior of the mechanism clutch-helical two stage gear. *Mechanism and Machine Theory*, *46*(7), 986–997. https://doi.org/10.1016/j.mechmachtheory.2011.02.002